Vorticity generation by short-crested wave breaking

David B. Clark,[1] Steve Elgar,[1] and Britt Raubenheimer[1]

Received 26 September 2012; revised 14 November 2012; accepted 16 November 2012; published 21 December 2012.

[1] Eddies and vortices associated with breaking waves rapidly disperse pollution, nutrients, and terrestrial material along the coast. Although theory and numerical models suggest that vorticity is generated near the ends of a breaking wave crest, this hypothesis has not been tested in the field. Here we report the first observations of wave-generated vertical vorticity (e.g., horizontal eddies), and find that individual short-crested breaking waves generate significant vorticity [$O(0.01\ s^{-1})$] in the surfzone. Left- and right-handed wave ends generate vorticity of opposite sign, consistent with theory. In contrast to theory, the observed vorticity also increases inside the breaking crest, possibly owing to onshore advection of vorticity generated at previous stages of breaking or from the shape of the breaking region. Short-crested breaking transferred energy from incident waves to lower frequency rotational motions that are a primary mechanism for dispersion near the shoreline. **Citation:** Clark, D. B., S. Elgar, and B. Raubenheimer (2012), Vorticity generation by short-crested wave breaking, *Geophys. Res. Lett.*, *39*, L24604, doi:10.1029/2012GL054034.

1. Introduction

[2] The tremendous dissipation of wave energy in the surfzone (the region of depth-limited breaking near the shoreline) drives vigorous dispersion of bacteria [*Boehm et al.*, 2002], larvae [*Rilov et al.*, 2008], sediments, and other suspended material, with surfzone eddy diffusivities roughly 10 times larger than those measured seaward of the breaking region [*Fong and Stacey*, 2003; *Spydell et al.*, 2007; *Jones et al.*, 2008; *Spydell and Feddersen*, 2009; *Spydell et al.*, 2009; *Brown et al.*, 2009; *Clark et al.*, 2010, 2011]. Recent studies suggest these high diffusivities are generated primarily by low-frequency (0.030–0.001 Hz) quasi-2D horizontal eddies [*Spydell and Feddersen*, 2009; *Clark et al.*, 2010; *Clark et al.*, 2011]. This region of high diffusivity causes rapid dispersion within the surfzone over long $O(10^3$–10^4 m) alongshore distances and relatively short O(100 m) cross-shore distances, and results in material appearing to be "trapped" near the coast [*Grant et al.*, 2005; *Clark et al.*, 2010].

[3] Despite the importance of eddies and dispersion, there have been few, if any direct observations of surfzone vorticity, and there are no observations of vertical vorticity (e.g., horizontal eddies) generated by breaking waves (including whitecaps). Moreover, the mechanisms that transfer energy from incident swell and sea waves to lower frequency eddies are not well understood, and may include short-crested breaking [*Peregrine*, 1998; *Bühler and Jacobson*, 2001; *Bonneton et al.*, 2010], alongshore variation in bathymetrically-controlled breaking [*Kennedy et al.*, 2006; *Castelle et al.*, 2010], sheared alongshore currents [*Noyes et al.*, 2004], and wave-groups [*Long and Özkan-Haller*, 2009]. These mechanisms must be quantified to model the dispersion and transport of pollutants, sediments, nutrients, and other tracers near the shoreline.

[4] Breaking waves (Figure 1) dissipate energy while transferring momentum that forces water in the direction of wave propagation. In the surfzone the time-averaged wave-driven forcing raises water levels near the shoreline [*Longuet-Higgins and Stewart*, 1964] and, in the case of obliquely incident waves, drives alongshore currents [*Longuet-Higgins*, 1970]. However, the instantaneous forcing is composed of individual breaking waves that often are short-crested owing to the directional spread of the wave field [*Longuet-Higgins*, 1957], with crests from different directions interacting to create alongshore varying wave amplitudes. Thus, the wave field is spatially inhomogeneous over wave time and spatial scales, with the largest amplitude section of the wave breaking first, resulting in a breaking region with a finite alongshore extent (Figure 1).

[5] Here, the non-uniform forcing from individual short-crested waves that generates the rotational motions associated with dispersion is explored. It has been hypothesized that vorticity ω about a vertical axis (termed "vorticity" here) is generated by along-crest variations in the breaking force

$$\frac{d\omega}{dt} = -\frac{dF_{\mathrm{br}}}{dy_{\mathrm{c}}}, \tag{1}$$

where t is time, F_{br} is the breaking force, and y_{c} is the along-crest direction [*Peregrine*, 1998, 1999; *Bühler and Jacobson*, 2001; *Bonneton et al.*, 2010]. Thus, the maximum vorticity generation is likely to occur at the crest end $y_{\mathrm{c}} = 0$, where adjacent regions of breaking and non-breaking wave crest are assumed to form a large differential in forcing (Figure 2). The direction of the crest end is hypothesized to determine the sign of the generated vorticity, with left- (Figure 2a) and right-handed (Figure 2b) ends generating positive and negative vorticity, respectively. In agreement with this theory, numerical model simulations suggest that short-crested breaking waves can generate vorticity [*Bühler and Jacobson*, 2001; *Johnson and Pattiaratchi*, 2006; *Sullivan et al.*, 2007; *Bruneau et al.*, 2011], and that vorticity variance and dispersion increase with the number of crest ends [*Spydell and Feddersen*, 2009] (via directional spread). However, the magnitude and structure of this vorticity have

[1]Woods Hole Oceanographic Institution, Woods Hole, Massachusetts, USA.

Corresponding author: D. B. Clark, Woods Hole Oceanographic Institution, 266 Woods Hole Rd., Woods Hole, MA 02543, USA. (dclark@whoi.edu)

0094-8276/12/2012GL054034

Figure 1. Photograph of breaking waves (propagating toward the shore from lower-right to upper-left) showing the triangular patches of residual white foam marking the location where breaking occurred. As the waves break, they transfer momentum to the water column and generate vorticity. The initially small breaking region on the lower right expands as the wave moves toward shore on the upper left. This pattern is typical in the surfzone, with the shape of the triangle varying with wave conditions.

not been quantified, and the theories have not been tested with ocean observations.

2. Methods

[6] The vorticity generated by short-crested breaking waves was measured in an ocean surfzone using a novel circular array of current meters. Time-dependent Boussinesq simulations of surfzone waves and currents [*Feddersen et al.*, 2011; *Clark et al.*, 2011] indicate that a circular-shaped array of current meters reduces wave noise relative to that from a rectangular array. An array with 10 acoustic Doppler current meters (sample volumes 0.8 m above the seafloor) arranged in a 10-m diameter circle was deployed on an ocean beach in Duck, NC. The 10-m diameter was large enough to capture many individual crest ends, but not so large as to encompass multiple ends at one time. The array was deployed for 12 hours in 1.6-m mean water depth on the crest of an alongshore sandbar, and was always within the surfzone. The bathymetry was alongshore uniform over several hundred meters around the array, and the alongshore locations of wave breaking were not bathymetrically controlled. Waves were normally incident and directionally spread, and the wave conditions seaward of the surfzone were nearly constant. At the array the significant wave height H_{sig} varied with the tidally fluctuating water depth (Figure 3c), the directional spread [*Kuik et al.*, 1988] varied inversely with depth from 16° to 22° (possibly by wave current interaction [*Henderson et al.*, 2006]), the mean period was 8 s, and the hourly mean alongshore currents were weak (<0.08 m/s).

[7] Video observations were used to identify times when short-crested breaking occurred within or near the array. The crest end is defined at the location where the forward projecting edge of the wave first intersects the wave trough (plunging wave, where dissipation begins), or where the turbulent water on the front face of the wave first reaches its maximum extent in front of the wave (spilling wave, where dissipation appears to develop fully). A short-crested breaking event occurs at time t_0 when the crest bisects the array, and the only crests considered are those with a single well-developed breaking region within 20 m alongshore of the array.

[8] The mean (in space) vertical vorticity $\bar{\omega}$ within the array is estimated using Kelvin's circulation theorem $\bar{\omega} = A^{-1}\oint \mathbf{u} \cdot d\mathbf{l}$, where A is the area inside the array, $\mathbf{u}$ is the horizontal velocity vector estimated from the current meters, and $\mathbf{l}$ is the closed path around the perimeter of the array. The vorticity generated by a short-crested wave $\Delta\bar{\omega} = \bar{\omega}(t_0 + \Delta t) - \bar{\omega}(t_0)$, is the change in vorticity between the observation at time t_0 (when the crest bisects the array) and the observation at Δt later. The observations are grouped by the along-crest position y_c of the array center relative to the crest end (Figure 2c), with $y_c > 0$ in the breaking region and $y_c < 0$ in the non-breaking region of the crest.

[9] Two equations for the $\Delta\bar{\omega}$ generated by a single crest end crossing a rectangular region of the surfzone are derived from theory (Appendix A), and are similar to the equations for wave-averaged vorticity generation [*Bonneton et al.*, 2010]. The equations assume wave height and mean depth vary slowly over the cross-shore extent of the region, the along-crest transition from non-breaking to fully developed breaking occurs within the region, and that left- and right-handed wave ends produce positive and negative vorticity, respectively. A rectangular region simplifies the equations,

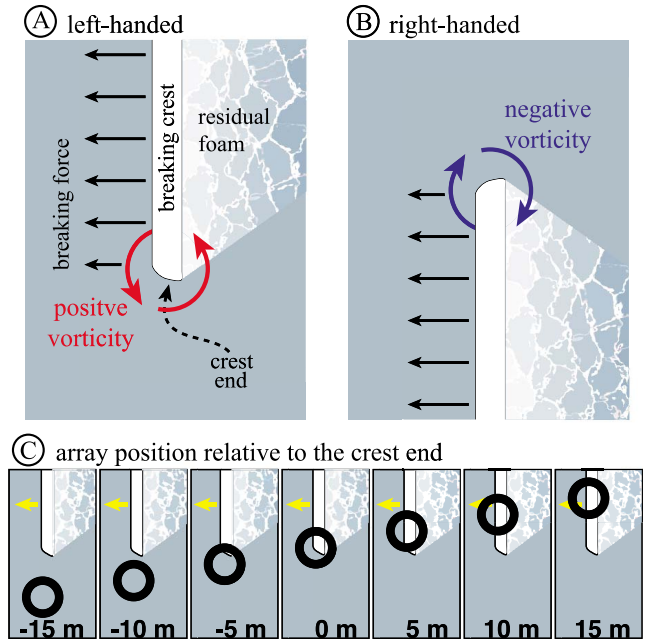

Figure 2. Schematic (looking down from above) of negative and positive vorticity generated by (a) left- and (b) right-handed ends of breaking waves. Solid black arrows indicate the instantaneous forcing (owing to breaking) on the water column in the direction of wave propagation, and the curved arrows indicate the direction of fluid rotation for the resulting positive (red) and negative (blue) vorticity. (c) Schematic of the vorticity array (black circle) position y_c relative to the crest-end with yellow arrows indicating the direction of wave propagation (left-handed example).

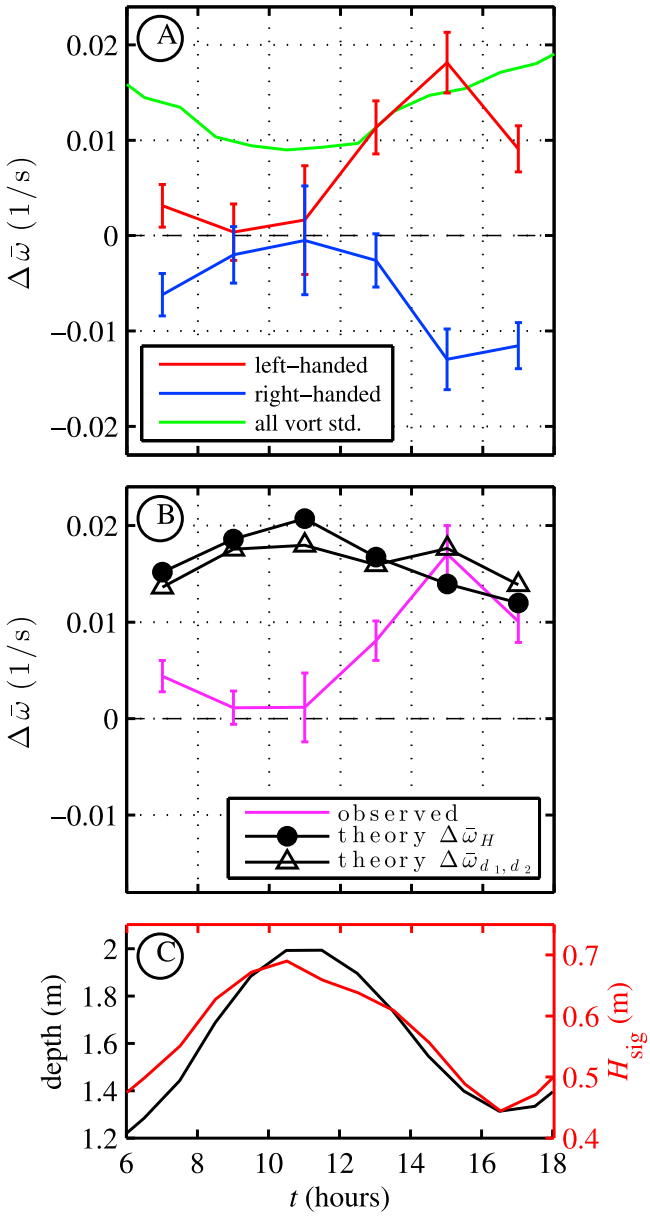

Figure 3. (a) Mean vorticity generated by (red curve) left- and (blue curve) right-handed short-crested waves versus time, with vertical bars indicating the error in the mean for each bin, and total vorticity standard deviation (green curve) versus time. (b) Mean vorticity generated by a short-crested wave versus time from (magenta curve) observations, and from theory using (black curve with triangles) mean quantities (2) and (black curve with circles) individual wave depths (3). (c) Water depth (black curve) and significant wave height H_{sig} (red curve), 4 times the standard deviation of the sea-surface-elevation fluctuations, versus time.

and the results are similar to those for a circular region with similar dimensions. Using mean quantities

$$\Delta\bar{\omega}_H \approx \pm \frac{3g^{\frac{1}{2}}}{8\Delta y} \frac{H^3(x_0)}{h^{\frac{5}{2}}(x_0)}, \qquad (2)$$

where H is the wave height, g is gravitational acceleration, h is the mean water depth, Δy is the alongshore length of the averaging region, and x_0 is at the center of the averaging region. A similar equation based on hydraulic jump equations is

$$\Delta\bar{\omega}_{d_1,d_2} \approx \pm \frac{3h}{4\Delta y} \frac{(d_2-d_1)^3}{(d_1 d_2)^{\frac{3}{2}}} \left[\frac{g}{2(d_1+d_2)}\right]^{\frac{1}{2}}, \qquad (3)$$

where d_1 and d_2 are the water depths on the low and high sides of the hydraulic jump, respectively.

3. Results and Discussion

[10] The variation in short-crested vorticity over a tidal cycle (Figure 3) is estimated from the average of waves with $5 \le y_c \le 10$ m and $3 \le \Delta t \le 18$ s. These averaging parameters span the maximum $\Delta\bar{\omega}$ (discussed below), and the range of values is used to increase the number of waves averaged. The observed $\Delta\bar{\omega}$ is positive for left-handed and negative for right-handed wave ends, in agreement with theory [*Peregrine*, 1998, 1999], and the temporal variations in left- and right-handed $\Delta\bar{\omega}$ are similar (Figure 3a). The $\Delta\bar{\omega}$ magnitudes are maximum near low tide and minimum near high tide. At low tide the array is farther inside the surfzone, with a larger region of breaking offshore, and at high tide the array is near the outer edge of the surfzone where waves begin to break. The variation in vorticity may be caused by greater total wave energy dissipated on the sandbar at low tide, or $\Delta\bar{\omega}$ may be cross-shore variable with greater $\Delta\bar{\omega}$ in the inner surfzone, possibly owing to a longer time history of breaking (see below).

[11] There were similar numbers of left- and right-handed crests, and the mean wave direction was near zero relative to shore normal. Under these conditions short-crested breaking is expected to produce vorticity variation, but little or no mean vorticity. Consistent with expectations, hourly mean vorticity (not shown) is on average 20% of the vorticity standard deviation (Figure 3a). During low tide individual waves produce $\Delta\bar{\omega}$ with magnitude equal to the vorticity standard deviation (Figure 3a, t = 16 hours), suggesting that short-crested breaking is a significant source of vorticity variation in the surfzone. The $O(0.01\ s^{-1})$ $\Delta\bar{\omega}$ observed here (Figure 3a) is similar to the modeled near-surface vorticity immediately after a single breaking event in the open ocean [*Sullivan et al.*, 2007], and to the modeled vorticity generated near a surfzone crest end [*Johnson and Pattiaratchi*, 2006].

[12] The observed $\Delta\bar{\omega}$ is compared with theory using equations (2) and (3) (Figure 3b), where $\Delta\bar{\omega}$ from left-handed waves is combined with $-\Delta\bar{\omega}$ from right-handed waves. The alongshore length of the averaging region Δy = 8.9 m is the length of the side of a square with an area equal to the 10 m diameter circular array. The observations are estimated from a subset of the waves, with a bias towards larger waves. Thus, for comparison with the observations, $\Delta\bar{\omega}_{d_1,d_2}$ (3) is estimated from the crest (d_2) and trough (d_1) depths for each wave used in the observational estimate, and $\Delta\bar{\omega}_H$ (2) is estimated from 2 hour mean wave heights $H = \langle d_2 - d_1 \rangle_t$, where $\langle\rangle_t$ is a time average. The $\Delta\bar{\omega}_H$ and the binned mean $\Delta\bar{\omega}_{d_1,d_2}$ are similar, and closely match the observed $\Delta\bar{\omega}$ at low tide (Figure 3b). However, $\Delta\bar{\omega}_H$ and $\Delta\bar{\omega}_{d_1,d_2}$ are larger than $\Delta\bar{\omega}$ at high tide when the array is in the outer surfzone and the assumption of well-developed

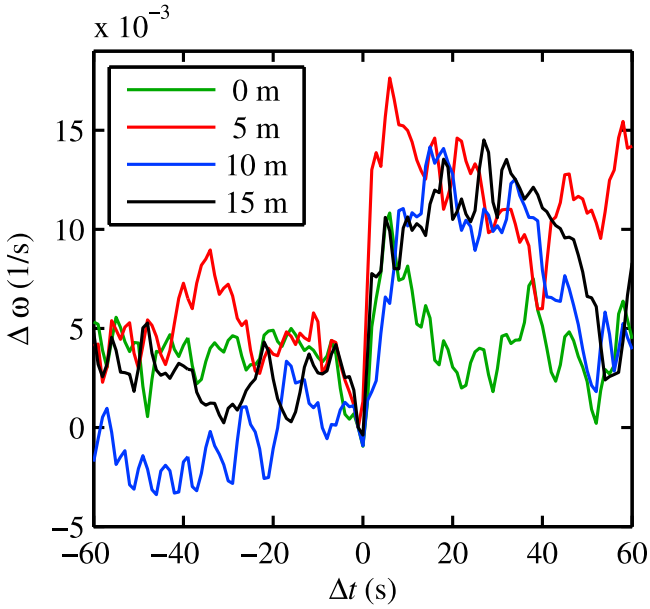

Figure 4. Change in vorticity associated with short-crested breaking versus time at four along-crest positions (see legend). Time $\Delta t = 0$ is when the crest bisects the array. The error in the mean ranges from ± 0.002 to ± 0.004 with smaller errors near $\Delta t = 0$ and larger errors at large Δt. Locations -15 to -5 m (outside the breaking crest, Figure 2c) are not shown because there is no significant change in vorticity.

breaking may be violated. The differences between theoretical (equations (2) and (3)) and observed vorticity may result from physical processes not included in the theoretical estimates.

[13] The structure of short-crested vorticity is explored by examining $\Delta\bar{\omega}$ over a range of Δt and y_c (Figure 4). Waves are averaged over low tides (Figure 3, $6 < t < 8$ and $13 < t <$ 18 hours) when $\Delta\bar{\omega}$ is greatest, and $\Delta\bar{\omega}$ from left-handed waves is combined with $-\Delta\bar{\omega}$ from right-handed waves. Before the short-crested breaking event ($\Delta t < 0$) the $\Delta\bar{\omega}$ are noisy with no significant change, whereas after the event ($\Delta t > 0$) there is a rapid increase in $\Delta\bar{\omega}$ at all $y_c \geq 0$ (Figure 4) with a maximum $\Delta\bar{\omega} = 0.018$ s^{-1} at $y_c = 5$ m and $\Delta t = 5$ s. For $y_c < 0$ (not shown) there is no significant change in $\Delta\bar{\omega}$ owing to the breaking event at $\Delta t = 0$.

[14] The generation of vorticity at $y_c = 10$ and 15 m (Figure 4, blue and black curves) is not predicted by (1) and the assumption that $\frac{dF_{br}}{dy_c}$ is maximum at the crest end, and may result from onshore advection of vorticity generated at previous stages of breaking or from the shape of the breaking region. For a directionally spread wave field on an ocean beach the breaking region of a wave rarely maintains its alongshore length, but starts as an initially narrow region of breaking in the outer surfzone and spreads alongshore as it propagates shoreward. This spreading can be seen in the triangular region of foam left in the wake of a breaking wave (Figure 1), where the foam indicates the region of forcing over the breaking history of the wave. The cross-shore integrated forcing is greatest near the alongshore center of the triangle, and decreases towards the alongshore ends. It is possible that this alongshore spreading of the breaking region generates vorticity along the entire breaking crest, except at the center of the triangle where the alongshore gradient in cross-shore integrated forcing is zero. Vorticity generated by triangular breaking regions is consistent with the increased $\Delta\bar{\omega}$ observed in the inner surfzone (low tide, Figure 3a), where waves have a longer time history of breaking.

[15] The time delay of the initial increase in $\Delta\bar{\omega}$ (Figure 4), which occurs over $0 < \Delta t < 5$ s at all $y_c > 0$, may be caused by near-surface forcing propagating downwards through the water column and the roughly 2.5 s for a wave to cross the array. The subsequent slow rise to maximum $\Delta\bar{\omega}$ at $\Delta t = 20$ s for $y_c = 10$ and 15 m is consistent with onshore advection of vorticity generated at previous stages of breaking, or the slow spin-up of larger scale vorticity owing to the triangular shape of the breaking region (Figure 1). The $\Delta\bar{\omega}$ generated by a short-crested wave decays over 20 to 60 s, with the most rapid decay at $y_c = 0$, and some evidence of persistent $\Delta\bar{\omega}$ over longer times at $y_c = 5$ m. The $\Delta\bar{\omega}$ decay may be caused by the advection of the wave-generated vorticity out of the sample region, the reduction of $\Delta\bar{\omega}$ through bottom friction, or the reversal of local vorticity by subsequent breaking events of opposite sign.

[16] Short-crested waves that crossed the array in roughly 2.5 s produced vorticity that persisted for 40 to 60 s (Figure 4), much longer than the 8 s mean period of the waves. Thus, momentum from waves with relatively high frequencies (0.12 Hz mean frequency) is being transferred into rotational motions with much lower frequencies. These lower-frequency rotational motions have been indicated as a primary cross-shore dispersion mechanism [*Spydell and Feddersen*, 2009; *Clark et al.*, 2010, 2011] and a primary alongshore dispersion mechanism when alongshore currents are weak [*Spydell and Feddersen*, 2009].

Appendix A

[17] Assuming an alongshore uniform beach and normally incident waves, the mean depth-averaged cross-shore breaking force f_{br} is

$$f_{br} = -\frac{1}{h}\frac{dS_{xx}}{dx}, \tag{A1}$$

where h is the mean depth and S_{xx} is the cross-shore (x) radiation stress [*Longuet-Higgins and Stewart*, 1964]. Assuming that the spatial derivative can be transformed to a temporal derivative using the bore velocity c_b gives (similar to *Bonneton et al.* [2010])

$$f_{br} = -\frac{1}{hc_b}\frac{d}{dt}\frac{3}{2}E = \frac{3}{2}\frac{D}{hc_b}, \tag{A2}$$

where t is time, E is the mean wave energy, and D is the mean depth-integrated dissipation. Assuming the total cross-shore forcing owing to a wave passing a point in space is Tf_{br}, where T is the wave period, and assuming the breaking force $F_{br}(x,y) = f_{br}(x)B(y)$ is separable, where $B(y)$ is a dimensionless function ranging from 0 to 1 that simulates the transition from non-breaking ($B = 0$) to fully developed breaking ($B = 1$), and integrating (1), the change in vorticity owing to a single breaking wave is

$$\Delta\omega = -Tf_{br}\frac{dB}{dy}. \tag{A3}$$

[18] Averaging (A3) over a rectangular region with sides Δx and Δy gives the change in mean vorticity owing to a single breaking wave

$$\Delta\bar{\omega} = \frac{1}{\Delta x \Delta y}\int_{x_0-\frac{\Delta x}{2}}^{x_0+\frac{\Delta x}{2}}\int_{y_0-\frac{\Delta y}{2}}^{y_0+\frac{\Delta y}{2}} T f_{\mathrm{br}}\frac{dB}{dy}\,dy dx, \tag{A4}$$

where (x_0, y_0) is the center of the array. Assuming the transition from non-breaking to fully developed breaking occurs within the alongshore extent of the averaging region (i.e., the integral of $\frac{dB}{dy}$ equals ± 1 depending on the crest end direction), and assuming variables of x are slowly varying over the cross-shore extent of the array,

$$\Delta\bar{\omega} \approx \pm\frac{1}{\Delta y} T(x_0) f_{\mathrm{br}}(x_0). \tag{A5}$$

[19] Substituting the mean breaking dissipation given by $D = \frac{gH^3}{4hT}$ [*Thornton and Guza*, 1983] into (A1) and (A4), and approximating the bore velocity as the linear wave speed, $c_{\mathrm{b}} = \sqrt{gh}$, gives the change in vorticity based on mean quantities

$$\Delta\bar{\omega}_H \approx \pm\frac{3g^{\frac{1}{2}}}{8\Delta y}\frac{H^3(x_0)}{h^{\frac{5}{2}}(x_0)}, \tag{A6}$$

where H is the wave height.

[20] A similar expression is derived from hydraulic jump equations [*Stive*, 1984], where the total dissipation across the hydraulic jump is

$$\mathfrak{D} = \frac{g c_{\mathrm{j}} h}{4}\frac{(d_2-d_1)^3}{d_1 d_2}, \tag{A7}$$

where d_1 and d_2 are the water depths on either side of the hydraulic jump and the hydraulic jump speed c_{j} is

$$c_{\mathrm{j}} = \left[\frac{g d_1 d_2 (d_2+d_1)}{2h^2}\right]^{\frac{1}{2}}. \tag{A8}$$

[21] Following (A1)–(A5) and equating $c_b TD$ with $\mathfrak{D}$, the change in vorticity based on depths from an individual wave is

$$\Delta\bar{\omega}_{d_1,d_2} \approx \frac{3h}{4\Delta y}\frac{(d_2-d_1)^3}{(d_1 d_2)^{\frac{3}{2}}}\left[\frac{g}{2(d_1+d_2)}\right]^{\frac{1}{2}}. \tag{A9}$$

[22] **Acknowledgments.** We thank Levi Gorrell, Danik Forsman, Christen Rivera-Erick, Regina Yopak, and Seth Zippel for their hard work in the field and the staff of the US Army Corps of Engineers Field Research Facility, Duck, NC for excellent logistical support. Funding was provided by a National Security Science and Engineering Faculty Fellowship, the Office of Naval Research, and a Woods Hole Oceanographic Institution Postdoctoral Fellowship.

[23] The Editor thanks two anonymous reviewers for assistance evaluating this paper.

References

Boehm, A. B., S. B. Grant, J. H. Kim, S. L. Mowbray, C. D. McGee, C. D. Clark, D. M. Foley, and D. E. Wellman (2002), Decadal and shorter period variability of surf zone water quality at Huntington Beach, California, *Environ. Sci. Technol.*, *36*, 3885–3892, doi:10.1021/es020524u.

Bonneton, P., N. Bruneau, B. Castelle, and F. Marche (2010), Large-scale vorticity generation due to dissipating waves in the surf zone, *Discrete Contin. Dyn. Syst., Ser. B*, *13*, 729–738, doi:10.3934/dcds2010.13.729.

Brown, J., J. H. MacMahan, A. Reneirs, and E. B. Thornton (2009), Surf zone diffusivity on a rip channeled beach, *J. Geophys. Res.*, *114*, C11015, doi:10.1029/2008JC005158.

Bruneau, N., P. Bonneton, B. Castelle, and R. Pedros (2011), Modeling rip current circulations and vorticity in a high-energy mesotidal-macrotidal environment, *J. Geophys. Res.*, *116*, C07026, doi:10.1029/2010JC006693.

Bühler, O., and T. E. Jacobson (2001), Wave-driven currents and vortex dynamics on barred beaches, *J. Fluid Mech.*, *449*, 313–339, doi:10.1017/S0022112001006322.

Castelle, B., H. Michallet, V. Marieu, F. Leckler, B. Dubardier, A. Lambert, C. Berni, P. Bonneton, E. Barthélemy, and F. Bouchette (2010), Laboratory experiment on rip current circulations over a moveable bed: Drifter measurements, *J. Geophys. Res.*, *115*, C12008, doi:10.1029/2010JC006343.

Clark, D. B., F. Feddersen, and R. T. Guza (2010), Cross-shore surfzone tracer dispersion in an alongshore current, *J. Geophys. Res.*, *115*, C10035, doi:10.1029/2009JC005683.

Clark, D. B., F. Feddersen, and R. T. Guza (2011), Modeling surfzone tracer plumes: 2. Transport and dispersion, *J. Geophys. Res.*, *116*, C11028, doi:10.1029/2011JC007211.

Feddersen, F., D. B. Clark, and R. T. Guza (2011), Modeling surfzone tracer plumes: 1. Waves, mean currents, and low-frequency eddies, *J. Geophys. Res.*, *116*, C11027, doi:10.1029/2011JC007210.

Fong, D. A., and M. Stacey (2003), Horizontal dispersion of a near-bed coastal plume, *J. Fluid Mech.*, *489*, 239–267, doi:10.1017/S002211200300510X.

Grant, S. B., J. H. Kim, B. H. Jones, S. A. Jenkins, J. Wasyl, and C. Cudaback (2005), Surf zone entrainment, along-shore transport, and human health implications of pollution from tidal outlets, *J. Geophys. Res.*, *110*, C10025, doi:10.1029/2004JC002401.

Henderson, S. M., R. T. Guza, S. Elgar, and T. H. C. Herbers (2006), Refraction of surface gravity waves by shear waves, *J. Phys. Oceanogr.*, *36*, 629–635, doi:10.1175/JPO2890.1.

Johnson, D., and C. Pattiaratchi (2006), Boussinesq modelling of transient rip currents, *Coastal Eng.*, *53*, 419–439, doi:10.1016/j.coastaleng.2005.11.005.

Jones, N. L., R. J. Lowe, G. Pawlak, D. A. Fong, and S. G. Monismith (2008), Plume dispersion on a fringing coral reef system, *Limnol. Oceanogr.*, *53*, 2273–2286, doi:10.4319/lo.2008.53.5_part_2.2273.

Kennedy, A. B., M. Brocchini, L. Soldini, and E. Gutierrez (2006), Topographically controlled, breaking-wave-induced macrovortices. Part 2. Changing geometries, *J. Fluid Mech.*, *559*, 57–80, doi:10.1017/S0022112006009979.

Kuik, A. J., G. P. Van Vledder, and L. H. Holthuijsen (1988), A method for the routine analysis of pitch-and-roll buoy wave data, *J. Phys. Oceanogr.*, *18*, 1020–1034, doi:10.1175/1520-0485(1988)018<1020:AMFTRA>2.0.CO;2.

Long, J. W., and H. T. Özkan-Haller (2009), Low-frequency characteristics of wave group–forced vortices, *J. Geophys. Res.*, *114*, C08004, doi:10.1029/2008JC004894.

Longuet-Higgins, M. S. (1957), The statistical analysis of a random, moving surface, *Philos. Trans. R. Soc. London, Ser. A*, *249*, 321–387, doi:10.1098/rsta.1957.0002.

Longuet-Higgins, M. S. (1970), Longshore currents generated by obliquely incident sea waves, *J. Geophys. Res.*, *75*, 6778–6789, doi:10.1029/JC075i033p06778.

Longuet-Higgins, M. S., and R. W. Stewart (1964), Radiation stresses in water waves: A physical discussion with applications, *Deep Sea Res.*, *11*, 529–562, doi:10.1016/0011-7471(64)90001-4.

Noyes, T. J., R. T. Guza, S. Elgar, and T. H. C. Herbers (2004), Field observations of shear waves in the surf zone, *J. Geophys. Res.*, *109*, C01031, doi:10.1029/2002JC001761.

Peregrine, D. H. (1998), Surf zone currents, *Theor. Comput. Fluid Dyn.*, *10*, 295–309, doi:10.1007/s001620050065.

Peregrine, D. H. (1999), Large-scale vorticity generation by breakers in shallow and deep water, *Eur. J. Mech. B Fluids*, *18*, 403–408, doi:10.1016/S0997-7546(99)80037-5.

Rilov, G., S. E. Dudas, B. A. Menge, B. A. Grantham, J. Lubchenco, and D. R. Schiel (2008), The surf zone: A semi-permeable barrier to onshore recruitment of invertebrate larvae?, *J. Exp. Mar. Biol. Ecol.*, *361*, 59–74, doi:10.1016/j.jembe.2008.04.008.

Spydell, M. S., and F. Feddersen (2009), Lagrangian drifter dispersion in the surf zone: Directionally spread, normally incident waves, *J. Phys. Oceanogr.*, *39*, 809–830, doi:10.1175/2008JPO3892.1.

Spydell, M. S., F. Feddersen, R. T. Guza, and W. E. Schmidt (2007), Observing surf-zone dispersion with drifters, *J. Phys. Oceanogr.*, *37*, 2920–2939, doi:10.1175/2007JPO3580.1.

Spydell, M. S., F. Feddersen, and R. T. Guza (2009), Observations of drifter dispersion in the surfzone: The effect of sheared alongshore currents, *J. Geophys. Res.*, *114*, C07028, doi:10.1029/2009JC005328.

Stive, M. J. F. (1984), Energy dissipation in waves breaking on gentle slopes, *Coastal Eng.*, *8*, 99–127, doi:10.1016/0378-3839(84)90007-3.

Sullivan, P. P., J. C. McWilliams, and W. K. Melville (2007), Surface gravity wave effects in the oceanic boundary layer: Large-eddy simulation with vortex force and stochastic breakers, *J. Fluid Mech.*, *593*, 405–452, doi:10.1017/S002211200700897X.

Thornton, E. B., and R. T. Guza (1983), Transformation of wave height distribution, *J. Geophys. Res.*, *88*, 5925–5938, doi:10.1029/JC088iC10p05925.